AGU ADVANCING EARTH AND SPACE SCIENCES

Geophysical Research Letters

RESEARCH LETTER
10.1029/2023GL106767

Detection of Earthquake Infragravity and Tsunami Waves With Underwater Distributed Acoustic Sensing

Han Xiao[1,2], Zack J. Spica[3], Jiaxuan Li[2], and Zhongwen Zhan[2]

[1]Helmholtz Center Potsdam, German GeoResearch Center GFZ, Potsdam, Germany, [2]Seismological Laboratory, Division of Geological and Planetary Sciences, California Institute of Technology, Pasadena, CA, USA, [3]Department of Earth and Environmental Sciences, University of Michigan, Ann Arbor, MI, USA

Key Points:

- We try to use subsea Distributed Acoustic Sensing (DAS) to improve early warning systems for infragravity and tsunami waves
- The research focuses on detecting infragravity and tsunami waves triggered by earthquakes
- We have developed a method to detect long-wavelength tsunami signals by adjusting sensor spacing according to water depth

Supporting Information:

Supporting Information may be found in the online version of this article.

Correspondence to:

H. Xiao,
xiaohan@gfz-potsdam.de

Citation:

Xiao, H., Spica, Z. J., Li, J., & Zhan, Z. (2024). Detection of earthquake infragravity and tsunami waves with underwater distributed acoustic sensing. *Geophysical Research Letters*, *51*, e2023GL106767. https://doi.org/10.1029/2023GL106767

Received 10 OCT 2023
Accepted 15 JAN 2024

Author Contributions:

Conceptualization: Han Xiao
Data curation: Zack J. Spica
Formal analysis: Han Xiao
Funding acquisition: Zack J. Spica, Zhongwen Zhan
Investigation: Han Xiao, Zack J. Spica, Jiaxuan Li, Zhongwen Zhan
Methodology: Han Xiao, Zack J. Spica, Jiaxuan Li, Zhongwen Zhan
Project administration: Zhongwen Zhan
Resources: Han Xiao, Zack J. Spica, Jiaxuan Li, Zhongwen Zhan
Software: Han Xiao
Supervision: Zhongwen Zhan
Validation: Han Xiao
Visualization: Han Xiao
Writing – original draft: Han Xiao

Abstract Underwater Distributed Acoustic Sensing (DAS) utilizes optical fiber as a continuous sensor array. It enables high-resolution data collection over long distances and holds promise to enhance tsunami early warning capabilities. This research focuses on detecting infragravity and tsunami waves associated with earthquakes and understanding their origin and dispersion characteristics through frequency-wavenumber domain transformations and beamforming techniques. We propose a velocity correction method based on adjusting the apparent channel spacing according to water depth to overcome the challenge of detecting long-wavelength and long-period tsunami signals. Experimental results demonstrate the successful retrieval of infragravity and tsunami waves using a subsea optical fiber in offshore Oregon. These findings underscore the potential of DAS technology to complement existing infragravity waves detection systems, enhance preparedness, and improve response efforts in coastal communities. Further research and development in this field are crucial to fully utilize the capabilities of DAS for enhanced tsunami monitoring and warning systems.

Plain Language Summary Subsea Distributed Acoustic Sensing (DAS) uses optical fiber as an extensive sensor array for strain data collection over long distances. This study investigates its potential to augment infragravity waves warning systems by focusing on detecting infragravity waves and tsunamis induced by earthquakes. We developed a methodology that accounts for irregular sensor depths to enhance the detection of long-wavelength tsunamis. Our experimental validation demonstrates the successful detection of these waves through a subsea optical fiber. Therefore, this technology holds promise for fortifying existing infragravity waves warning systems and improving coastal preparedness.

1. Introduction

Tsunamis are ocean waves typically caused by underwater earthquakes, volcanic eruptions, or landslides. Tsunamis have caused significant loss of life and property throughout history (Carvajal et al., 2022; Harbitz et al., 2006; Kanamori, 1972; Mori et al., 2011; Omira et al., 2022; Ward, 2001) and continue to be one of the major hazards to coastal populations and infrastructures (Bryant, 2008; Horspool et al., 2014; Johnston et al., 2005; Salamon et al., 2007). Early detection and timely dissemination of accurate tsunami warnings can provide coastal communities with vital information to evacuate vulnerable areas, initiate emergency response procedures, and minimize casualties (Gonzalez et al., 1998; Lauterjung et al., 2010; Selva et al., 2021). A system that has demonstrated its effectiveness in enhancing global tsunami warning capabilities is the Deep-ocean Assessment and Reporting of Tsunamis (DART) system (Gonzalez et al., 1998). It consists of a sparse network of anchored ocean bottom pressure recorders (BPR) strategically placed across the world's oceans. A BPR continuously monitors and measures changes in oceanic pressure, which is transmitted to a moored buoy with telemetry providing crucial real-time data to coastal observatories (Gonzalez et al., 1998). While DART systems effectively meet their goals in sending accurate early warning alerts, maintaining the seafloor infrastructure and the associated surface buoys requires substantial and constant financial resources. Due to this poor scalability, the number of DART stations deployed globally is limited, resulting in coverage gaps in many regions.

In recent years, researchers have been exploring innovative approaches to enhance tsunami early warning capabilities (Chatfield et al., 2013; Schöne et al., 2011; Selva et al., 2021). One promising technology gaining attention is Distributed Acoustic Sensing (DAS) on subsea fiber-optic cables (Becerril et al., 2022). DAS utilizes the optical phase changes in Rayleigh backscattered light within an optical fiber to function as thousands of

Writing – review & editing: Han Xiao, Zack J. Spica, Jiaxuan Li, Zhongwen Zhan

vibration sensors. This innovative approach enables the fiber to act as a dense array capable of continuously detecting and analyzing seismo-acoustic signals along tens of kilometers (Farghal et al., 2022; Lindsey et al., 2019; Lior et al., 2021; Romanowicz et al., 2023; Sladen et al., 2019; Spica et al., 2020, 2022, 2023; Viens et al., 2023; Williams et al., 2019; Xiao et al., 2022; Yang et al., 2022; Zhan, 2019). Unlike traditional sensors, DAS provides high-resolution data over large distances, allowing for real-time monitoring of seismic and ocean waves with unprecedented coverage. In many regions of the world, DAS for tsunami early warning systems would offer the advantage of minimal installation costs due to the presence of an extensive network of submarine fibers that is the backbone of our modern telecommunication infrastructure.

Thus far and to the best of our knowledge, there have been no peer-reviewed reports of success in using DAS to detect tsunamis. This is primarily attributed to the currently limited number of long-term and continuous subsea DAS deployments and the lower observational sensitivity of individual DAS channels for long-period signals, including tsunamis, as their sensitivity rapidly decreases with decreasing frequencies (Costa et al., 2019; Hartog et al., 2018; Lindsey & Martin, 2021).

In this study, we propose an effective DAS signal processing method and report the first observation of infragravity (high-frequency tsunamis) and tsunami waves induced by earthquakes from ocean bottom DAS data (Bromirski & Stephen, 2012; Ito et al., 2020; Sementsov et al., 2019; Wei et al., 2018). In general, infragravity waves are surface gravity waves with frequencies lower than wind waves (Webb et al., 1991). They occupy the lower end of the oceanic wave spectrum, with a dominant frequency typically between 0.005 and 0.05 Hz (Herbers et al., 1994, 1995), and are primarily generated by nonlinear interactions between higher-frequency wind waves (Hasselmann et al., 1963; Longuet-Higgins & Stewart, 1962). Wind waves and ocean swells have shorter periods, typically ranging from 0.04 to 1 Hz, and are the dominating signal in subsea DAS studies (Lindsey et al., 2019; Williams et al., 2019; Xiao et al., 2022). Besides, the typical frequency band of tsunamis ranges from about 0.14 to 5 mHz (200–7,140 s). Previous research has identified tsunamis with higher frequencies, notably at 30 mHz (33.3 s) and up to 60 mHz (16.7 s) (Hanson et al., 2007; Rabinovich et al., 2013). However, in our study, signals exceeding 3.3 mHz (300 s) are classified as infragravity waves, following the definition established by Munk (1950).

2. Data

A FEBUS Optics A1-R interrogator unit (IU) was deployed to probe the first 60 km of the Alaska-Oregon Network telecommunication cable, starting from Florence, Oregon, between August 6 and 1 December 2021 (Figure 1). The instrument recorded strain-rate data in intervals of 20 m, using a gauge length of 40 m and a sampling frequency of 100 Hz, yielding an array of 3,000 channels. The recorded data are continuous, apart from a brief 3-day interruption from September 7 to September 10. Per the cable installation report, the initial 6.3 km of the cable connects the landing station to the coastline via a sequence of conduits running along roads (i.e., the first 315 channels). The succeeding 53.7 km of the probed segment lies offshore (i.e., 2,685 channels), buried beneath 80–100 cm of sediment. From 6.3 to 40 km from the IU, the cable is situated on the continental shelf in water less than ∼150 m deep. The seabed then drops from 150 to 400 m between 40 and 60 km from the interrogator, indicating the beginning of the continental slope. From the coastline, the mean azimuth of the cable is ∼254° from the north, representing a direction almost perpendicular to the mean shoreline orientation (Viens et al., 2023).

During this period, two tsunamis occurred (Figure 1a). One took place on 12 August 2021, triggered by a magnitude 8.1 earthquake in the South Sandwich Islands region (Jia et al., 2022). A tsunami with a maximum run-up height of approximately 75 cm was measured at King Edward Point, located on the South Georgia Islands. The tsunami signals were observed at various places, reaching King Cove, Alaska, with a run-up height of 15 cm (Titov et al., 2021). Another tsunami occurred on 8 September 2021, originating from a magnitude 7.0 earthquake in Guerrero, Mexico. In this event, a small tsunami measuring 37 cm was recorded in Guerrero. Unfortunately, the data from this second tsunami is incomplete as it overlaps with the 3-day data gap.

Additionally, we gathered the data from the National Oceanic and Atmospheric Administration (NOAA) for the specified period from the DART buoys 46,407 and 46,411. The data from these buoys are sampled at an interval of 15 s, and the water depths are 3,318 m and 4,328 m, respectively. Moreover, we collected data from the Crescent City, California, tide gauge with station code 9419750, which has a sampling interval of 1 min. We also utilized the ocean bottom pressure sensors NV.NCBC and NV.BACND from the NEPTUNE Canada underwater

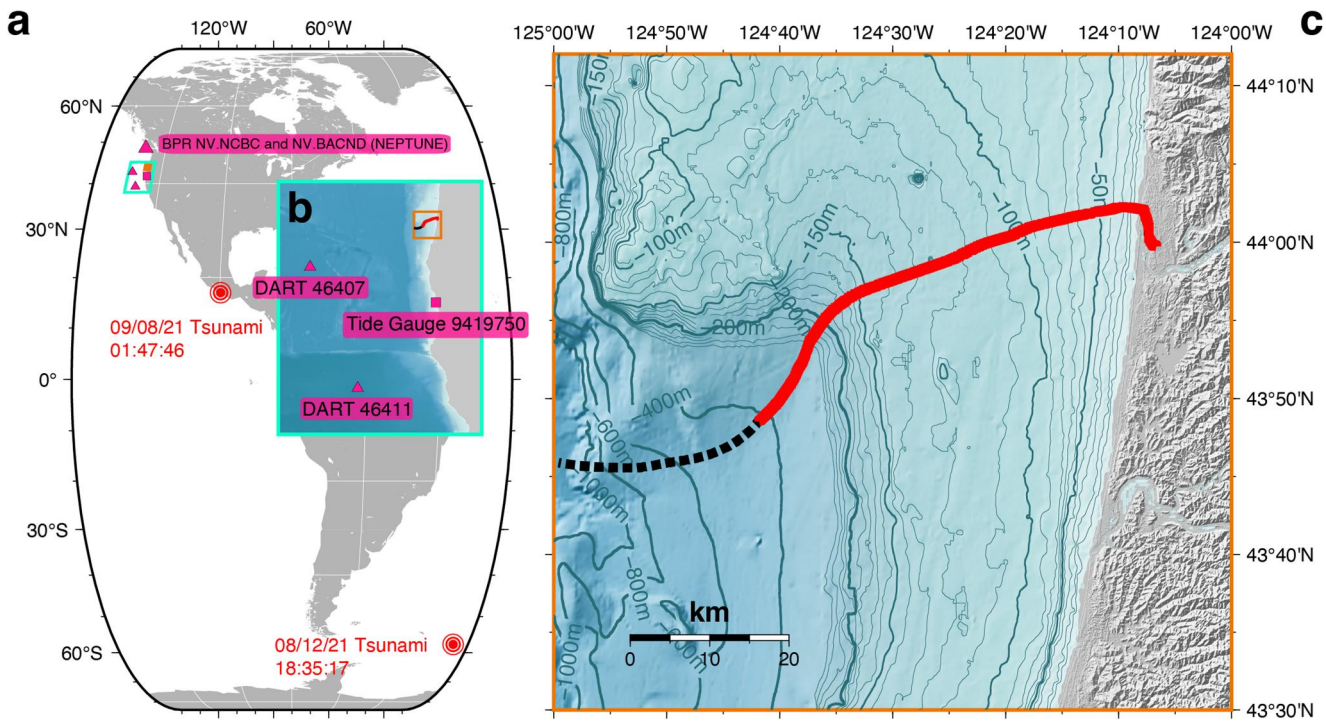

Figure 1. Locations of the subsea DAS (Distributed Acoustic Sensing) system, DART (Deep-ocean Assessment and Reporting of Tsunamis) observation systems, BPRs (bottom pressure recorders), tide gauge, and two tsunami events. Panel (b) indicated by the blue box in panel (a), shows the precise locations of the DART and tide gauge. Panel (c) zooms in on the red box in panel (b), revealing the water depth and position of the DAS system.

observatory records. Their respective water depths are 398 and 643 m, with a distance of 9.2 km between them. The sampling rate is 5 Hz. The locations of these instruments are shown in Figure 1b.

3. Methods

We first preprocess the data by down sampling the continuous strain-rate data to 1 Hz, applying spectral whitening, and removing the mean and trend. Then, we transform the entire subsea DAS data set with a one-hour step into the frequency-wavenumber (FK) domain (Spica et al., 2020; Williams et al., 2019). We analyze infragravity and tsunami waves, which follow the dispersion curve of gravity waves $\omega^2 = gk \tanh(kh)$ according to linear theory (Lighthill, 2001). Here, ω represents the angular frequency, g represents the acceleration due to gravity, k represents the wavenumber, and h represents the water depth. The stacked results of FK domain transformations for the entire 1-month data of August 2021 are presented in Figures 2a and 2b. The red dashed line in Figures 2a and 2b represents the dispersion curve corresponding to a water depth of 120 m; that is, the average DAS cable depth. In Figure 2a, the results highlight the presence of infragravity waves in the frequency band 0.005–0.03 Hz, whereas Figure 2b shows the frequency range encompassing both wind waves and microseisms (Lindsey et al., 2019; Williams et al., 2019; Xiao et al., 2018). In Figure 2b, the energy of the landward wind waves is 10 times greater than that of the seaward wind waves (Elgar et al., 1994). In contrast, for infragravity waves, the energy of the landward waves is approximately equal to that of the seaward waves. This observation suggests distinct characteristics in the energy distribution and behavior of different wave types.

From Figure 2, it is evident that the results of the FK transformation do not capture any signals below 5 mHz (above 200 s), which implies that directly applying the FK transformation cannot adequately capture the tsunami signal. This is due to the significant variation in the speed of tsunamis with water depth (Figure S1A in Supporting Information S1) and their long wavelengths (Figure S1B in Supporting Information S1). Longer optical fibers are required to effectively observe long-wavelength tsunamis, but this can lead to increased variations in water depth, resulting in greater differences in tsunami wave speeds. Performing the FK transformation directly is equivalent to applying the same speed time delay correction and stacking all channels together. Since tsunamis have different

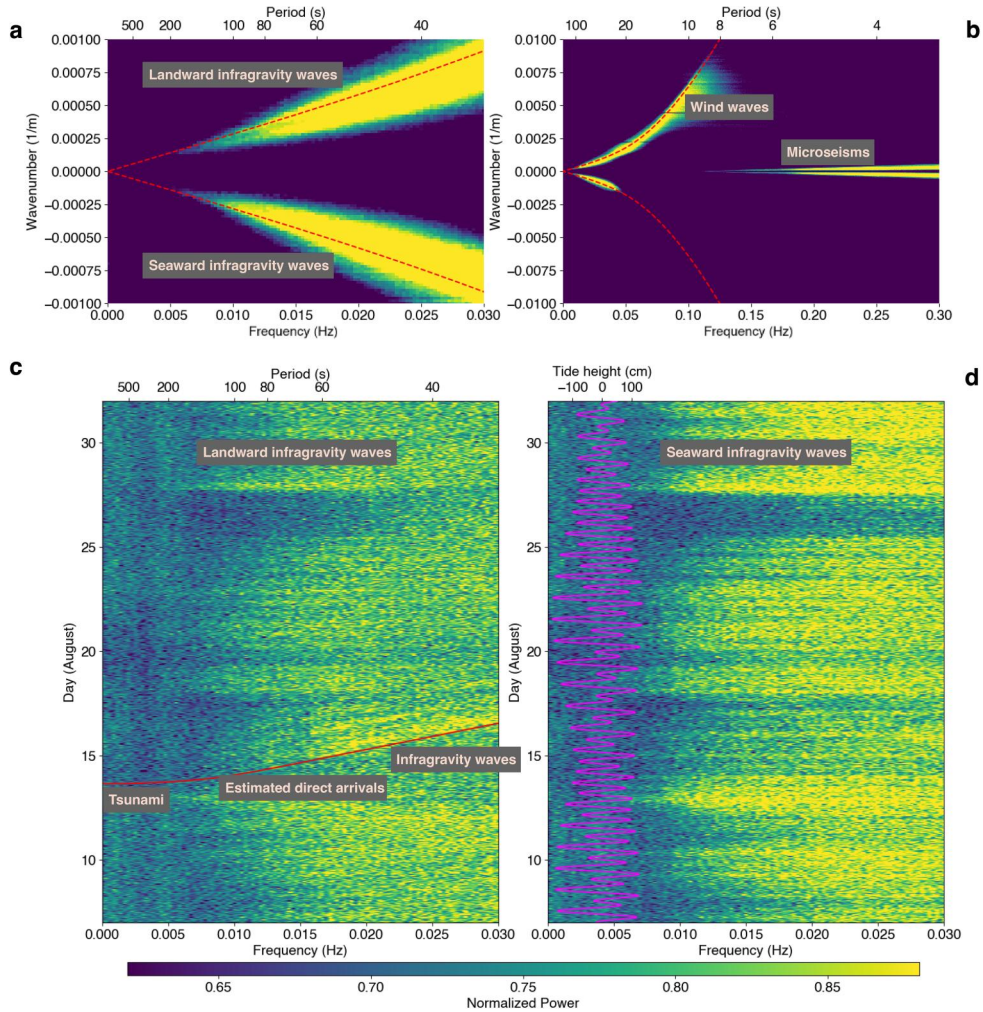

Figure 2. FK (frequency-wavenumber) transformation results are displayed in panels (a) and (b). Panel (a) presents the stacked results of the FK transformation for the entire month of August 2021, focusing on the frequency band associated with infragravity waves. Panel (b) showcases the frequency bands of wind waves and microseisms. The red dashed line in both panels corresponds to the theoretical result corresponding to a water depth of 120 m. Panels (c) and (d) illustrate the hourly variations of the FK results for the month of August 2021. Panel (c) shows landward waves, while panel (d) displays seaward waves. In panel (c), the solid red line indicates the estimated arrival time of the tsunami and infragravity waves generated by the magnitude 8.1 earthquake in the South Sandwich Islands. The purple line in panel (d) represents the calculated tide variations at the location of the DAS cable.

speeds at different water depths, this time delay correction according to one single speed is inaccurate and does not help stack the signals optimally.

For instance, consider infragravity waves with a 100-s period (10 mHz). At a depth of approximately 150 m, these waves have a wavelength of around 3.8 km. Therefore, a fiber optic section that spans 3.8 km is sufficient to detect such waves. Thus, the 33–40 km section of the fiber optic system, where the depth ranges between 130 and 150 m (and the velocity is between 35.4 and 37.9 m/s), is ideally configured to effectively capture the 100-s infragravity wave signal. In contrast, tsunami waves with a 1000-s period (1 mHz) have a much longer wavelength, exceeding 38.3 km at the same depth. This necessitates a fiber optic length of at least 38.3 km for reliable signal detection. However, for distances beyond 38.3 km, the detection of tsunami waves becomes impractical using FK transformation. This is due to significant variations in wave velocity caused by larger depth changes (ranging from 100 to 420 m over distances of 20–60 km, with velocities between 31.3 and 64.1 m/s).

Thus, we propose a simple method to correct the apparent speed of tsunamis to a uniform apparent speed by adjusting the spacing between channels based on the local water depth such as:

$$\frac{d_a}{d_r} = \frac{V_a}{\sqrt{\frac{g}{k}(\tanh(kh))}} \tag{1}$$

where d_a refers to the adjusted channel spacing, d_r represents the actual channel spacing, and V_a denotes the target corrected velocity. In situations where the optical fiber is deployed in deep water, where tsunamis propagate at higher speeds, we apply a shorter artificial spacing to the channels. This adjustment results in a reduction in the apparent speed of the tsunami waves. Conversely, for channels situated in shallow water, we assign them a longer artificial channel spacing, which amplifies the apparent speed. By assigning a uniform apparent speed to all channels - that is, 30 m/s - we can correct for the differences in speed that prevent the detection of long-period tsunami signals. Our simulation calculations also demonstrate the necessity of velocity adjustment for tsunami waves (Figures S2 and S3 in Supporting Information S1). At the same time, to facilitate result comparisons, we employed ArcGIS to calculate the theoretical arrival times of the tsunamis (Johnston et al., 2001).

4. Results

4.1. Infragravity Waves

By extracting the energy curve (Red line in Figure 2a) at varying frequencies every hour based on the local water depth, we can observe the infragravity waves for both landward and seaward waves (Figures 2c and 2d). In particular, we observe infragravity waves generated from two different regions. Locally, the variations in these background infragravity waves are closely linked to tidal changes, exhibiting no frequency dispersion features in shallow water (Figure 2 and Figure S1A in Supporting Information S1). In previous studies, researchers found that the observed strong tidal modulation of infragravity waves is caused by nonlinear energy transfers from these low-frequency long waves (infragravity waves) to higher-frequency motions. This energy transfer is particularly enhanced during low tide (Okihiro & Guza, 1995; Thomson et al., 2006). Infragravity waves with periods longer than 20 s is primarily generated locally from shorter-period wind waves (<20 s). This was evident from the strong correlation between the energy of infragravity waves and the short-period ocean waves recorded at local buoys (Dolenc et al., 2005; Elgar et al., 1992). Our findings also suggest that the generation of infragravity waves is concentrated in localized areas, and their predominant propagation occurs in shallow water regions. This behavior is attributed to the absence of frequency dispersion characteristics when the water depth is small (Figure S1A in Supporting Information S1). In these regions, infragravity waves exhibit insignificant frequency dispersion due to their characteristic as shallow-water waves. Additionally, in regions with shallow water depth where the wavelength (λ) considerably exceeds the depth ($\lambda \gg h$), the velocity of infragravity waves is notably influenced by the water's depth rather than the frequency of the waves (Figure S1A in Supporting Information S1). These observations shed light on the complex behavior of infragravity waves and their interaction with the surrounding environment.

In addition to the background infragravity waves, we observe the presence of infragravity waves originating from the deep ocean, characterized by noticeable frequency dispersion, where low-frequency infragravity waves travel faster (Figure 2c). The red line in Figure 2c represents the theoretical estimated arrival time of the infragravity and tsunami waves as if they were associated with the South Sandwich Islands region on 12 August 2021 (Figure 1a). We find that the calculated arrival time of the infragravity waves matches well with the observed first arrival time. Furthermore, the tsunami and infragravity waves generated by this earthquake were also recorded by the pressure sensors NV.NCBC and NV.BACND at the NEPTUNE Canada underwater observatory (Figure S4 in Supporting Information S1). To enhance our analysis, we utilize correlation information from these two distinct stations (Figures S4C and S4D in Supporting Information S1). Therefore, we conclude that the infragravity waves observed here were generated in conjunction with the earthquake, originating from the magnitude 8.1 earthquake in the South Sandwich Islands region. In addition, it is noteworthy that multiple subsequent arrivals of infragravity waves occur after the initial arrival (Figure 2c). These subsequent waves exhibit consistent dispersion characteristics, indicating that they originate from the same region. We hypothesize that these subsequent arrivals

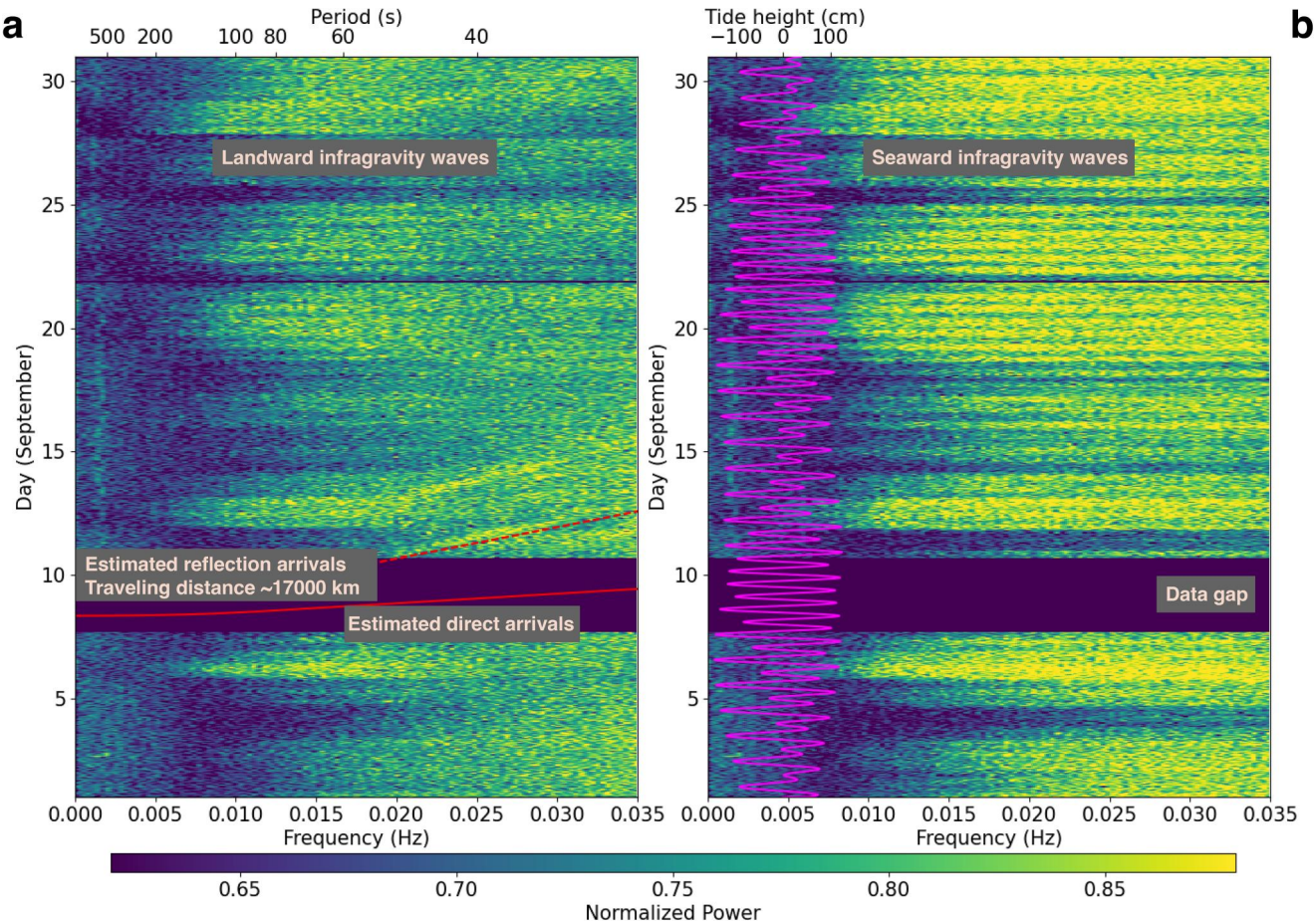

Figure 3. Similar to Figure 2, but for the month of September 2021. In panel (a), the solid red line represents the estimated arrival time of the tsunami and infragravity waves caused by the magnitude 7.0 earthquake in Guerrero. The red dashed lines represent the estimated arrival time of reflection waves at various frequencies when propagate 17,000 km.

may be attributed to the local or regional reflections of infragravity waves generated around the earthquake's epicenter. However, the exact cause is unclear and needs more investigation.

Due to data limitations, we are unable to detect the direct infragravity waves after the Guerrero earthquake (Figure 3). However, similarly to the South Sandwich event, we detect significant reflection infragravity wave (Red dash line) energy reaching the DAS array after the theoretical first arrival (Red solid line). The temporal characteristics of these waves align well with expectations. Indeed, according to the frequency dispersion curve, the propagation distance of these infragravity waves appeared to be approximately 17,000 km. However, the actual geographical distance between Guerrero, Mexico, and the DAS array in Oregon is about 5,200 km. Hence, our interpretation points toward a reflection of the infragravity waves, presumably originating from the Samoa islands or Iturup islands in the Pacific Ocean. According to this interpretation, these waves appear to have traveled 17,000 km before reaching the DAS cable in Oregon (Figure S5 in Supporting Information S1).

Additionally, 57.6 hr after the first reflected infragravity waves, we observe another burst of infragravity wave energy. Because this train of infragravity wave share similar dispersion features, the distance from their source to the fiber must be similar. Yet no major aftershock was recorded, and the origin of these waves is unknown. This observation underscores the complexity of wave propagation and highlights the importance of considering multiple factors when analyzing such phenomena.

At the same time, it is worth mentioning that during October and November, when no tsunamis occurred, we do not observe any infragravity waves propagating from the deep ocean (Figures S6 and S7 in Supporting Information S1).

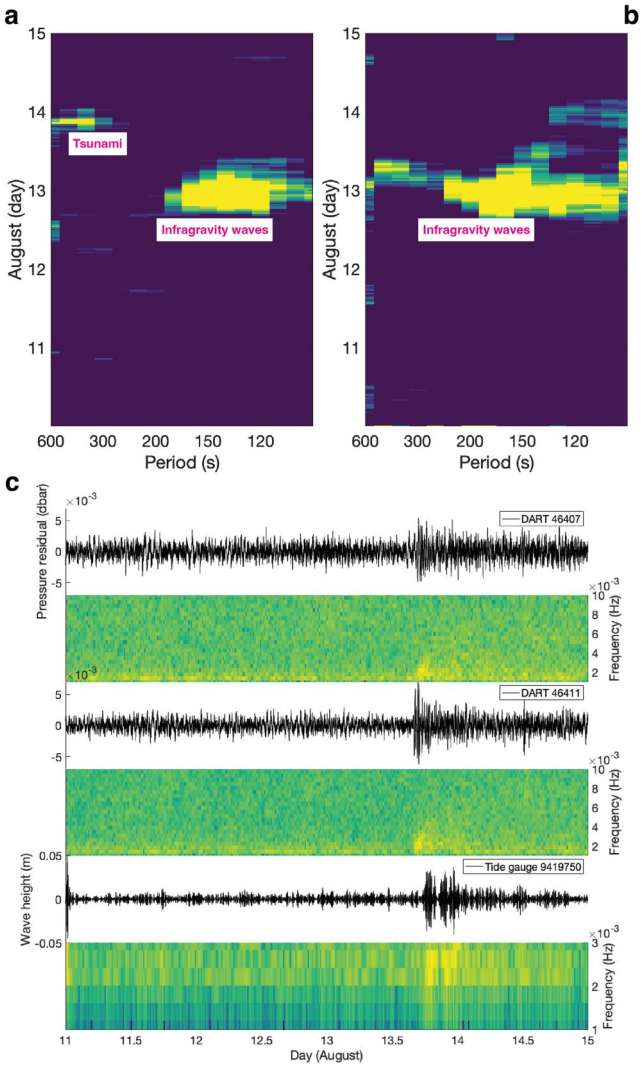

Figure 4. The FK beamforming results of tsunami and infragravity waves, after applying the velocity adjustment, are presented in panels (a) and (b), representing the landward waves, and seaward waves, respectively. Panel (c) shows the recorded waveforms and its spectrums of tsunami waves from the South Sandwich Islands region, obtained from the DART and tide gauge systems.

4.2. Earthquake Tsunami Detection

After performing the channel spacing adjustment, we can then use the FK beamforming method (Capon, 1969; Gal et al., 2014) to analyze the data and search for ocean wave signals with periods greater than 300 s. Figure S8 in Supporting Information S1 illustrates the one-hour results obtained at the different periods for the time of 17:30 on 13 August 2021. Figures 4a and 4b display the results of the corrected beamforming analysis at different periods and times. We observe that the signals of infragravity waves can now be detected in the range of 200–600 s (1.67–5 mHz), compared to the FK transformation results before the adjustment (Figures 2c and 2d). Additionally, and most importantly, we can observe a signal at the predicted tsunami arrival time and align it with the tsunami wave arrivals recorded by the DART and the tide gauge (Figure 4c). Nonetheless, these findings require additional validation through the analysis of more examples using the subsea DAS system. Unfortunately, due to a data gap during the latter event, we cannot record the direct arrivals for the tsunami originating from Guerrero.

5. Discussion and Conclusions

We investigate the potential of subsea DAS systems to enhance tsunami early warning capabilities. The DART system, consisting of seafloor bottom pressure recorders, has been effective in global tsunami warning systems but is limited by high costs and coverage gaps. DAS, utilizing telecom optical fiber as a continuous sensor, offers high-resolution data over large distances, making it a promising technology for real-time monitoring of tsunami waves.

Previous studies found that tsunamis have the potential to induce infragravity waves (Bromirski & Stephen, 2012). Ito et al. (2020) also observed anomalous infragravity waves at sites offshore of New Zealand's North Island, coinciding with the arrival of Rayleigh waves. These ultra-low-frequency waves had a similar amplitude to the subsequent tsunami generated by the earthquakes. The researchers found that the amplitude of the observed waves varied with water depth, indicating that infragravity waves were likely excited by Rayleigh or Love waves amplified within the accretionary wedge offshore. Therefore, we can utilize infragravity waves as an indicator for coastal tsunamis, as both infragravity waves and tsunamis propagate at the same speed in shallow coastal areas (Figure S1A in Supporting Information S1), even in situations where the sensitivity of DAS to long-period tsunami signals is low.

At the same time, the detection and monitoring of infragravity waves itself play a crucial role in coastal hazard management and safety. These infragravity waves, often generated by the swell in the shallow water (Longuet-Higgins & Stewart, 1962), can pose a threat to coastal areas (Hattori et al., 2020; Matsuba et al., 2020). They frequently contribute to coastal flooding, erosion, sediment transport, and the formation of dangerous rip currents (Beach & Sternberg, 1988; Bertin et al., 2018; Osborne & Greenwood, 1992; Sheremet et al., 2014; Zheng et al., 2021). By understanding and analyzing the characteristics of infragravity waves, such as their amplitude, frequency, and propagation patterns, coastal authorities and communities can enhance their ability to predict and mitigate the impacts of these waves. Early detection of infragravity waves can facilitate timely evacuation plans, implementation of coastal defenses, and issuing appropriate warnings to ensure the safety of coastal residents and visitors.

However, currently, infragravity waves cannot leave clear indications on the BPRs if their wavelength surpasses twice the water depth. For instance, in an average ocean depth lower than 3 km (i.e., the average depth of DART systems), this translates to infragravity waves with frequencies below 16 mHz and wavelengths of 6 km. Despite being aware of the presence of infragravity waves on the ocean's surface, their direct measurement above 16 mHz using DART systems is impossible due to the aforementioned filtering effect.

This study shows that we can detect infragravity waves using subsea DAS while they approach the continental shelf (Figures 2 and 3). Through FK domain transformations, we observe infragravity waves originating from earthquakes. In the case of the South Sandwich Islands earthquake, the observed infragravity waves align with the theoretically estimated arrival time, indicating their association with the tsunami generated by the earthquake. Additionally, as depicted in Figure 2, the energy of the infragravity waves induced by the earthquake in the South Sandwich Islands, which reached the DAS cable after propagating over 17,500 km, remained comparable to the background energy levels. This suggests that infragravity waves generated in the vicinity of the seismic event potentially exhibit significantly higher energy levels than background infragravity waves. Hence, this could potentially serve as an indication of an impending tsunami event. In the case of the Guerrero tsunami, limitations in the available data prevent us from observing direct infragravity waves. However, we do detect significant reflection infragravity waves.

During F-K transformation calculations, we use a half-hour long time series from different channels to perform an FK transformation. For infragravity waves with a period of 100 s, we can derive the corresponding signals even with 20 or 10 min of data. Transmitting low-sample-rate data (e.g., with a 10-s sampling rate) is fast, even with 3,000 channels of data. Moreover, the computational time needed for the F-K transformation is negligible (e.g., <2 s). Given the usual time frame of up to 1 hour for infragravity waves to reach coastal areas, the proposed method enables early detection, thereby enhancing its efficacy in providing advance warnings.

Besides, our understanding of how earthquakes precisely excite infragravity waves remains limited. To gain a more comprehensive understanding of the mechanisms behind infragravity wave generation by earthquakes, further data collection and extensive theoretical research are required. Combining these data with advanced theoretical models can lead to a more accurate understanding of the mechanisms involved in generating infragravity waves during seismic activities. Ongoing efforts to study and unravel the complexities of infragravity wave generation will be crucial in effectively managing coastal hazards and ensuring the safety and resilience of vulnerable coastal regions.

Underwater pressure gauge arrays often detect more subtle signals (Kubota et al., 2020), offering insights into the sources and characteristics of various oceanic waves (Kohler et al., 2020; Tonegawa et al., 2018). These tools have been crucial in advancing our comprehension of oceanographic phenomena. Currently, DAS technology provides a compelling solution to obtain high-fidelity and dense marine observations. It represents a low-cost alternative when compared to recent ocean-bottom pressure networks like NEPTUNE in Canada (Barnes et al., 2015) and Japan's S-net and DONET (Kaneda et al., 2015). Consequently, this study not only illuminates the mechanisms of infragravity wave generation but also paves the way for new opportunities in oceanographic research.

Furthermore, to address the challenge of detecting long-period tsunami signals, we develop a velocity adjustment method that corrects the spacing between channels based on water depths. By applying this correction and utilizing FK beamforming, we can detect tsunami and infragravity waves at periods greater than 300 s (Figure 4 and Figure S8 in Supporting Information S1). The arrival times of the tsunami align with those recorded by DART and tide gauge measurements, suggesting it is possible to use subsea DAS to capture direct waves of tsunamis. Nevertheless, additional validation is necessary, which can be achieved by analyzing more examples using the subsea DAS system.

Overall, this study highlights the potential of DAS technology in enhancing infragravity and tsunami waves early warning systems. By providing unprecedented coverage and real-time monitoring capabilities, DAS systems have the potential to complement existing tsunami detection systems and improve preparedness and response efforts in coastal communities. Further research and development in this field are crucial to fully harness the capabilities of DAS for enhanced tsunami monitoring and warning systems. This research has the potential to lay the groundwork for future advancements in this field.

Data Availability Statement

The BPRs data of NEPTUNE used in this study were collected from the Incorporated Research Institutions for Seismology (IRIS) Data Management Center (DMC; https://ds.iris.edu/mda/NV/). The DART data are from National Oceanic and Atmospheric Administration (NOAA, https://www.ngdc.noaa.gov/thredds/catalog/dart_bpr/processed/catalog.html). The tide gauge data 9419750 at Crescent City is also NOAA but in a different

website (https://tidesandcurrents.noaa.gov/waterlevels.html?id=9419750). The bathymetry data is downloaded from https://www.gebco.net/data_and_products/gridded_bathymetry_data/. All data needed to evaluate the conclusions in the paper are present in the paper and/or the Supporting Information S1. Three days of DAS data including the tsunami and infragravity waves shown in Figures 2–4 are accessible on Zenodo (Spica et al., 2023; Xiao & Spica, 2024).

Acknowledgments
The authors extend their gratitude to Editor Daoyuan Sun and the anonymous reviewers for their invaluable suggestions and inputs. The authors would like to thank Loïc Viens, Mohan Pan for their helpful suggestions. This work was supported by the Gordon Moore Foundation #9500 and National Science Foundation CAREER award 1848166. Z.J.S acknowledges support from the NSF award EAR2022716.

References

Barnes, C. R., Best, M. M. R., Johnson, F. R., & Pirenne, B. (2015). NEPTUNE Canada: Installation and initial operation of the world's first regional cabled ocean observatory. In *Seafloor observatories: A new vision of the Earth from the Abyss* (pp. 415–438). Springer Berlin Heidelberg. https://doi.org/10.1007/978-3-642-11374-1_16

Beach, R. A., & Sternberg, R. W. (1988). Suspended sediment transport in the surf zone: Response to cross-shore infragravity motion. *Marine Geology*, *80*(1), 61–79. https://doi.org/10.1016/0025-3227(88)90072-2

Becerril, C., Vidal-Moreno, P. J., Sladen, A., Ampuero, J.-P., & Gonzalez-Herraez, M. (2022). *Towards tsunami early-warning with distributed acoustic sensing (DAS)*. AGU Fall Meeting Abstracts. ID S16A-07.

Bertin, X., de Bakker, A., van Dongeren, A., Coco, G., André, G., Ardhuin, F., et al. (2018). Infragravity waves: From driving mechanisms to impacts. *Earth-Science Reviews*, *177*, 774–799. https://doi.org/10.1016/j.earscirev.2018.01.002

Bromirski, P. D., & Stephen, R. A. (2012). Response of the Ross Ice shelf, Antarctica, to ocean gravity-wave forcing. *Annals of Glaciology*, *53*(60), 163–172. https://doi.org/10.3189/2012AoG60A058

Bryant, E. (2008). *Tsunami-the underrated hazard*. Springer. https://doi.org/10.1007/978-3-540-74274-6

Capon, J. (1969). High-resolution frequency-wavenumber spectrum analysis. *Proceedings of the IEEE*, *57*(8), 1408–1418. https://doi.org/10.1109/PROC.1969.7278

Carvajal, M., Sepúlveda, I., Gubler, A., & Garreaud, R. (2022). Worldwide signature of the 2022 Tonga volcanic tsunami. *Geophysical Research Letters*, *49*(6), e2022GL098153. https://doi.org/10.1029/2022GL098153

Chatfield, A. T., Scholl, H. J., & Brajawidagda, U. (2013). Tsunami early warnings via Twitter in government: Net-savvy citizens' co-production of time-critical public information services. *Government Information Quarterly*, *30*(4), 377–386. https://doi.org/10.1016/j.giq.2013.05.021

Costa, L., Martins, H. F., Martín-López, S., Fernández-Ruiz, M. R., & González-Herráez, M. (2019). Fully distributed optical fiber strain sensor with 10−12 $\epsilon/\sqrt{\text{Hz}}$ sensitivity. *Journal of Lightwave Technology*, *37*(18), 4487–4495. https://doi.org/10.1109/JLT.2019.2904560

Dolenc, D., Romanowicz, B., Stakes, D., McGill, P., & Neuhauser, D. (2005). Observations of infragravity waves at the Monterey ocean bottom broadband station (MOBB). *Geochemistry, Geophysics, Geosystems*, *6*(9). https://doi.org/10.1029/2005GC000988

Elgar, S., Herbers, T. H. C., & Guza, R. T. (1994). Reflection of ocean surface gravity waves from a Natural Beach. *Journal of Physical Oceanography*, *24*(7), 1503–1511. https://doi.org/10.1175/1520-0485(1994)024<1503:ROOSGW>2.0.CO;2

Elgar, S., Herbers, T. H. C., Okihiro, M., Oltman-Shay, J., & Guza, R. T. (1992). Observations of infragravity waves. *Journal of Geophysical Research*, *97*(C10), 15573–15577. https://doi.org/10.1029/92JC01316

Farghal, N. S., Saunders, J. K., & Parker, G. A. (2022). The potential of using fiber optic distributed acoustic sensing (DAS) in earthquake early warning applications. *Bulletin of the Seismological Society of America*, *112*(3), 1416–1435. https://doi.org/10.1785/0120210214

Gal, M., Reading, A. M., Ellingsen, S. P., Koper, K. D., Gibbons, S. J., & Näsholm, S. P. (2014). Improved implementation of the fk and Capon methods for array analysis of seismic noise. *Geophysical Journal International*, *198*(2), 1045–1054. https://doi.org/10.1093/gji/ggu183

Gonzalez, F. I., Milburn, H. M., Bernard, E. N., & Newman, J. C. (1998). Deep-ocean assessment and reporting of tsunamis (DART): Brief overview and status report. *Proceedings of the International Workshop on Tsunami Disaster Mitigation*.

Hanson, J. A., Reasoner, C. L., & Bowman, J. R. (2007). High-frequency tsunami signals of the great Indonesian earthquakes of 26 December 2004 and 28 March 2005. *Bulletin of the Seismological Society of America*, *97*(1A), S232–S248. https://doi.org/10.1785/0120050607

Harbitz, C. B., Løvholt, F., Pedersen, G., & Masson, D. G. (2006). Mechanisms of tsunami generation by submarine landslides: A short review. *Norwegian Journal of Geology/Norsk Geologisk Forening*, *86*(3).

Hartog, A. H., Belal, M., & Clare, M. A. (2018). Advances in distributed fiber-optic sensing for monitoring marine infrastructure, measuring the deep ocean, and quantifying the risks posed by seafloor hazards. *Marine Technology Society Journal*, *52*(5), 58–73. https://doi.org/10.4031/MTSJ.52.5.7

Hasselmann, K., Munk, W., & MacDonald, G. (1963). Bispectra of ocean waves. In *Symposium on time series analysis*.

Hattori, N., Tajima, Y., Yamanaka, Y., & Kumagai, K. (2020). Study on the influence of infragravity waves on inundation characteristics at Minami-Ashiyahama in Osaka Bay induced by the 2018 Typhoon Jebi. *Coastal Engineering Journal*, *62*(2), 182–197. https://doi.org/10.1080/21664250.2020.1724247

Herbers, T., Elgar, S., & Guza, R. (1994). Infragravity-frequency (0.005–0.05 Hz) motions on the shelf. Part I: Forced waves. *Journal of Physical Oceanography*, *24*(5), 917–927. https://doi.org/10.1175/1520-0485(1994)024<0917:IFHMOT>2.0.CO;2

Herbers, T., Elgar, S., Guza, R., & O'Reilly, W. (1995). Infragravity-frequency (0.005–0.05 Hz) motions on the shelf. Part II: Free waves. *Journal of Physical Oceanography*, *25*(6), 1063–1079. https://doi.org/10.1175/1520-0485(1995)025<1063:IFHMOT>2.0.CO;2

Horspool, N., Pranantyo, I., Griffin, J., Latief, H., Natawidjaja, D. H., Kongko, W., et al. (2014). A probabilistic tsunami hazard assessment for Indonesia. *Natural Hazards and Earth System Sciences*, *14*(11), 3105–3122. https://doi.org/10.5194/nhess-14-3105-2014

Ito, Y., Webb, S. C., Kaneko, Y., Wallace, L. M., & Hino, R. (2020). Sea surface gravity waves excited by dynamic ground motions from large regional earthquakes. *Seismological Research Letters*, *91*(4), 2268–2277. https://doi.org/10.1785/0220190267

Jia, Z., Zhan, Z., & Kanamori, H. (2022). The 2021 South Sandwich island Mw 8.2 earthquake: A slow event sandwiched between regular ruptures. *Geophysical Research Letters*, *49*(3), e2021GL097104. https://doi.org/10.1029/2021GL097104

Johnston, D., Paton, D., Crawford, G. L., Ronan, K., Houghton, B., & Bürgelt, P. (2005). Measuring tsunami preparedness in coastal Washington, United States. *Natural Hazards*, *35*(1), 173–184. https://doi.org/10.1007/s11069-004-2419-8

Johnston, K., Ver Hoef, J. M., Krivoruchko, K., & Lucas, N. (2001). *Using ArcGIS geostatistical analyst* (Vol. 380). Esri Redlands.

Kanamori, H. (1972). Mechanism of tsunami earthquakes. *Physics of the Earth and Planetary Interiors*, *6*(5), 346–359. https://doi.org/10.1016/0031-9201(72)90058-1

Kaneda, Y., Kawaguchi, K., Araki, E., Matsumoto, H., Nakamura, T., Kamiya, S., et al. (2015). Development and application of an advanced ocean floor network system for megathrust earthquakes and tsunamis. In P. Favali, L. Beranzoli, & A. De Santis (Eds.), *Seafloor observatories: A new vision of the Earth from the Abyss* (pp. 643–662). Springer Berlin Heidelberg. https://doi.org/10.1007/978-3-642-11374-1_25

Kohler, M. D., Bowden, D. C., Ampuero, J.-P., & Shi, J. (2020). Globally scattered 2011 Tohoku tsunami waves from a seafloor sensor array in the Northeast Pacific ocean. *Journal of Geophysical Research: Solid Earth*, *125*(11), e2020JB020221. https://doi.org/10.1029/2020JB020221

Kubota, T., Saito, T., & Suzuki, W. (2020). Millimeter-scale tsunami detected by a wide and dense observation array in the deep ocean: Fault modeling of an Mw 6.0 interplate earthquake off Sanriku, NE Japan. *Geophysical Research Letters*, *47*(4), e2019GL085842. https://doi.org/10.1029/2019GL085842

Lauterjung, J., Münch, U., & Rudloff, A. (2010). The challenge of installing a tsunami early warning system in the vicinity of the Sunda Arc, Indonesia. *Natural Hazards and Earth System Sciences*, *10*(4), 641–646. https://doi.org/10.5194/nhess-10-641-2010

Lighthill, J. (2001). *Waves in fluids*. Cambridge university press. https://doi.org/10.1088/0957-0233/13/9/707

Lindsey, N. J., Dawe, T. C., & Ajo-Franklin, J. B. (2019). Illuminating seafloor faults and ocean dynamics with dark fiber distributed acoustic sensing. *Science*, *366*(6469), 1103–1107. https://doi.org/10.1126/science.aay5881

Lindsey, N. J., & Martin, E. R. (2021). Fiber-optic Seismology. *Annual Review of Earth and Planetary Sciences*, *49*(1), 309–336. https://doi.org/10.1146/annurev-earth-072420-065213

Lior, I., Sladen, A., Rivet, D., Ampuero, J.-P., Hello, Y., Becerril, C., et al. (2021). On the detection capabilities of underwater distributed acoustic sensing. *Journal of Geophysical Research: Solid Earth*, *126*(3), e2020JB020925. https://doi.org/10.1029/2020JB020925

Longuet-Higgins, M. S., & Stewart, R. W. (1962). Radiation stress and mass transport in gravity waves, with application to 'surf beats. *Journal of Fluid Mechanics*, *13*(4), 481–504. https://doi.org/10.1017/S0022112062000877

Matsuba, Y., Shimozono, T., & Sato, S. (2020). Infragravity wave dynamics on Seisho Coast during Typhoon Lan in 2017. *Coastal Engineering Journal*, *62*(2), 299–316. https://doi.org/10.1080/21664250.2020.1753901

Mori, N., Takahashi, T., Yasuda, T., & Yanagisawa, H. (2011). Survey of 2011 Tohoku earthquake tsunami inundation and run-up. *Geophysical Research Letters*, *38*(7). https://doi.org/10.1029/2011GL049210

Munk, W. H. (1950). Origin and generation of waves. *Coastal Engineering Proceedings*, *1*(1), 1. https://doi.org/10.9753/icce.v1.1

Okihiro, M., & Guza, R. T. (1995). Infragravity energy modulation by tides. *Journal of Geophysical Research*, *100*(C8), 16143–16148. https://doi.org/10.1029/95JC01545

Omira, R., Ramalho, R. S., Kim, J., González, P. J., Kadri, U., Miranda, J. M., et al. (2022). Global Tonga tsunami explained by a fast-moving atmospheric source. *Nature*, *609*(7928), 734–740. https://doi.org/10.1038/s41586-022-04926-4

Osborne, P. D., & Greenwood, B. (1992). Frequency dependent cross-shore suspended sediment transport. 2. A barred shoreface. *Marine Geology*, *106*(1), 25–51. https://doi.org/10.1016/0025-3227(92)90053-K

Rabinovich, A. B., Thomson, R. E., & Fine, I. V. (2013). The 2010 Chilean tsunami off the west coast of Canada and the Northwest Coast of the United States. *Pure and Applied Geophysics*, *170*(9), 1529–1565. https://doi.org/10.1007/s00024-012-0541-1

Romanowicz, B., Allen, R., Brekke, K., Chen, L. W., Gou, Y., Henson, I., et al. (2023). SeaFOAM: A year-long DAS deployment in Monterey Bay, California. *Seismological Research Letters*, *94*(5), 2348–2359. https://doi.org/10.1785/0220230047

Salamon, A., Rockwell, T., Ward, S. N., Guidoboni, E., & Comastri, A. (2007). Tsunami hazard evaluation of the eastern Mediterranean: Historical analysis and selected modeling. *Bulletin of the Seismological Society of America*, *97*(3), 705–724. https://doi.org/10.1785/0120060147

Schöne, T., Pandoe, W., Mudita, I., Roemer, S., Illigner, J., Zech, C., & Galas, R. (2011). GPS water level measurements for Indonesia's Tsunami Early Warning System. *Natural Hazards and Earth System Sciences*, *11*(3), 741–749. https://doi.org/10.5194/nhess-11-741-2011

Selva, J., Lorito, S., Volpe, M., Romano, F., Tonini, R., Perfetti, P., et al. (2021). Probabilistic tsunami forecasting for early warning. *Nature Communications*, *12*(1), 5677. https://doi.org/10.1038/s41467-021-25815-w

Sementsov, K. A., Nosov, M. A., Kolesov, S. V., Karpov, V. A., Matsumoto, H., & Kaneda, Y. (2019). Free gravity waves in the ocean excited by seismic surface waves: Observations and numerical simulations. *Journal of Geophysical Research: Oceans*, *124*(11), 8468–8484. https://doi.org/10.1029/2019JC015115

Sheremet, A., Staples, T., Ardhuin, F., Suanez, S., & Fichaut, B. (2014). Observations of large infragravity wave runup at Banneg Island, France. *Geophysical Research Letters*, *41*(3), 976–982. https://doi.org/10.1002/2013GL058880

Sladen, A., Rivet, D., Ampuero, J. P., De Barros, L., Hello, Y., Calbris, G., & Lamare, P. (2019). Distributed sensing of earthquakes and ocean-solid Earth interactions on seafloor telecom cables. *Nature Communications*, *10*(1), 5777. https://doi.org/10.1038/s41467-019-13793-z

Spica, Z. J., Ajo-Franklin, J., Beroza, G. C., Biondi, B., Cheng, F., Gaite, B., et al. (2023). PubDAS: A PUBlic distributed acoustic sensing datasets repository for geosciences. *Seismological Research Letters*, *94*(2A), 983–998. https://doi.org/10.1785/0220220279

Spica, Z. J., Castellanos, J. C., Viens, L., Nishida, K., Akuhara, T., Shinohara, M., & Yamada, T. (2022). Subsurface imaging with ocean-bottom distributed acoustic sensing and water phases reverberations. *Geophysical Research Letters*, *49*(2), e2021GL095287. https://doi.org/10.1029/2021GL095287

Spica, Z. J., Nishida, K., Akuhara, T., Pétrélis, F., Shinohara, M., & Yamada, T. (2020). Marine sediment characterized by ocean-bottom fiber-optic Seismology. *Geophysical Research Letters*, *47*(16), e2020GL088360. https://doi.org/10.1029/2020GL088360

Thomson, J., Elgar, S., Raubenheimer, B., Herbers, T. H. C., & Guza, R. T. (2006). Tidal modulation of infragravity waves via nonlinear energy losses in the surfzone. *Geophysical Research Letters*, *33*(5). https://doi.org/10.1029/2005GL025514

Titov, V., Sannikova, N., Arcas, D., Moore, C., & Wei, Y. (2021). *South Sandwich Islands tsunami: Observation and modeling*. AGU Fall Meeting Abstracts. ID S42C-10.

Tonegawa, T., Fukao, Y., Shiobara, H., Sugioka, H., Ito, A., & Yamashita, M. (2018). Excitation location and seasonal variation of transoceanic infragravity waves observed at an absolute pressure gauge array. *Journal of Geophysical Research: Oceans*, *123*(1), 40–52. https://doi.org/10.1002/2017JC013488

Viens, L., Spica, Z. J., Delbridge, B. G., & Arbic, B. K. (2023). Monitoring shelf sea dynamics with ocean-bottom distributed acoustic sensing. *ESS Open Archive*. https://doi.org/10.22541/essoar.167898504.40579102/v1

Ward, S. N. (2001). Landslide tsunami. *Journal of Geophysical Research*, *106*(B6), 11201–11215. https://doi.org/10.1029/2000JB900450

Webb, S. C., Zhang, X., & Crawford, W. (1991). Infragravity waves in the deep ocean. *Journal of Geophysical Research*, *96*(C2), 2723–2736. https://doi.org/10.1029/90JC02212

Wei, Y., Bromirski, P. D., Arcas, D., & Dunham, E. M. (2018). *Propagation of tsunami-induced infragravity waves*. AGU Fall Meeting Abstracts. ID NH41C-0989.

Williams, E. F., Fernández-Ruiz, M. R., Magalhaes, R., Vanthillo, R., Zhan, Z., González-Herráez, M., & Martins, H. F. (2019). Distributed sensing of microseisms and teleseisms with submarine dark fibers. *Nature Communications*, *10*(1), 5778. https://doi.org/10.1038/s41467-019-13262-7

Xiao, H., & Spica, Z. J. (2024). DAS Data for Detection of earthquake infragravity and tsunami waves with underwater distributed acoustic sensing [Dataset]. Zenodo. https://doi.org/10.5281/zenodo.10463888

Xiao, H., Tanimoto, T., Spica, Z. J., Gaite, B., Ruiz-Barajas, S., Pan, M., & Viens, L. (2022). Locating the precise sources of high-frequency microseisms using distributed acoustic sensing. *Geophysical Research Letters*, *49*(17), e2022GL099292. https://doi.org/10.1029/2022GL099292

Xiao, H., Xue, M., Yang, T., Liu, C., Hua, Q., Xia, S., et al. (2018). The characteristics of microseisms in South China Sea: Results from a combined data set of OBSs, broadband land seismic stations, and a global wave height model. *Journal of Geophysical Research: Solid Earth*, *123*(5), 3923–3942. https://doi.org/10.1029/2017JB015291

Yang, Y., Atterholt, J. W., Shen, Z., Muir, J. B., Williams, E. F., & Zhan, Z. (2022). Sub-kilometer correlation between near-surface structure and ground motion measured with distributed acoustic sensing. *Geophysical Research Letters*, *49*(1), e2021GL096503. https://doi.org/10.1029/2021GL096503

Zhan, Z. (2019). Distributed acoustic sensing turns fiber-optic cables into sensitive seismic Antennas. *Seismological Research Letters*, *91*(1), 1–15. https://doi.org/10.1785/0220190112

Zheng, Z., Ma, X., Ma, Y., Huang, X., & Dong, G. (2021). Modeling of coastal infragravity waves using the spectral model WAVEWATCH III. *Coastal Engineering*, *170*, 104016. https://doi.org/10.1016/j.coastaleng.2021.104016